PHOTONICS Research

Sculpturing spatiotemporal wavepackets with chirped pulses

Qian Cao,[1] Jian Chen,[1] Keyin Lu,[1] Chenhao Wan,[1,2] Andy Chong,[3,4] and Qiwen Zhan[1,*]

[1]School of Optical-Electrical and Computer Engineering, University of Shanghai for Science and Technology, Shanghai 200093, China
[2]School of Optical and Electronic Information, Huazhong University of Science and Technology, Wuhan 430074, China
[3]Department of Physics, University of Dayton, Dayton, Ohio 45469, USA
[4]Department of Electro-Optics and Photonics, University of Dayton, Dayton, Ohio 45469, USA
*Corresponding author: qwzhan@usst.edu.cn

Received 6 August 2021; revised 21 September 2021; accepted 21 September 2021; posted 21 September 2021 (Doc. ID 439849); published 26 October 2021

Pulse shaping has become a powerful tool in generating complicated ultrafast optical waveforms to meet specific application needs. Traditionally, pulse shaping focuses on the temporal waveform synthesis. Recent interests in structuring light in the spatiotemporal domain rely on Fourier analysis. A space-to-time mapping technique allows us to directly imprint complex spatiotemporal modulation through taking advantage of the relationship between frequency and time of chirped pulses. The concept is experimentally verified through the generation of spatiotemporal optical vortex (STOV) and STOV lattice. The power of this method is further demonstrated by STOV polarity reversal, vortex collision, and vortex annihilation. Such a direct mapping technique opens tremendous potential opportunities for sculpturing complex spatiotemporal waveforms.

https://doi.org/10.1364/PRJ.439849

1. INTRODUCTION

With the rapid advances made in laser technology, ultrafast lasers are widely available and making great impacts in many scientific disciplines and industrial applications. Complementary pulse shaping techniques have been developed to synthesize complicated optical waveforms to meet specific application needs. Among various pulse shaping techniques, pulse shapers based on spatial light modulators (SLMs) are the most attractive due to their programmability and versatility [1]. In a typical pulse shaper, SLM can also be replaced with metasurface devices to provide comprehensive modulation as opposed to phase only or amplitude only modulation [2]. Most pulse shaping studies focus on the temporal waveform and take unchirped pulses as the input, or, in the case where chirped pulses were used, the SLM in the pulse shaper will be programmed to compress the pulse and then generate the prescribed waveform in the temporal domain.

Spatiotemporal (ST) coupling, namely the coupling between spatial or spatial-frequency and temporal or frequency coordinates, is well known in ultrafast optics, particularly as the pulse width gets shorter. In general, ST coupling is considered to be detrimental in ultrafast laser applications. However, recently, it has been discovered that ST wavepackets (STWPs) have unique properties through intentional engineering of the space–time coupling. For example, pulse wavefront tilt [3] of a chirped pulse has been exploited in "attosecond lighthouse" for attosecond pulse generation [4]. ST intensity shaping has led to 3D lithographic microfabrication [5], the discoveries of light bullet [6], and diffraction-free space–time light sheets [7]. A combination of chromatic aberration with temporal chirp has enabled advanced control of the velocity of the intensity peak formed by a laser pulse [8] and led to the realization of so-called "flying focus" [9]. Precisely engineered ST spectral correlations may lead to anomalous refraction that defies expectations from Fermat's principle [10]. Most recently, the ST phase control enabled the generation of an ST optical vortex (STOV) [11,12] that carries purely transverse orbital angular momentum (OAM).

An efficient way to introduce controllable ST coupling is to apply modulation in the frequency domain within a typical 4-f pulse shaper through loading a spatial phase/amplitude pattern on the SLM. This has been evolving into a very powerful tool to generate STWPs with a variety of unusual properties. However, the connection between the spatial modulation on the SLM and the desired ST distribution can be more subtle, as the coordinates involved are not independent, and the fields in different domains are generally related through Fourier transforms. It does not offer an intuitive way to design more complicated sculpturing [13]. Thus, it is highly desirable if direct mapping can be realized so that the desired amplitude and/or phase modulation can be imposed on wavepackets in the ST domain.

2. METHODS

Here, we demonstrate that such a direct mapping can be realized through the use of chirped pulses as the input into a pulse shaper (we will call this STWP generator). Direct space (frequency) to time mapping is realized through taking advantage of the linear time dependence of the instantaneous frequency contained within the chirped pulse. We demonstrate its capability through generating STWPs with various prescribed structures. Let us take an ultrafast pulse with positive chirp as an example. This type of pulse is very common from many ultrafast pulse lasers. Assuming a Gaussian profile in both the spatial and temporal domains, the input pulse can be expressed as

$$E_i(x,y,z,t) = u(x,y)A(t)e^{i(\omega_0 t-kz)}e^{-\frac{t^2}{\tau^2}}e^{-\frac{iat^2}{\tau^2}}, \quad a>0. \tag{1}$$

For such a pulse, the instantaneous frequency can be found as

$$\omega(t) = \omega_0 - 2at/\tau^2. \tag{2}$$

Clearly, in this case, the instantaneous frequency is linearly related to time. After the grating, different frequency is dispersed along the y direction, where the diffraction angle of each frequency is $\theta(\omega) \cong \alpha\omega$, with α determined by the dispersion of the grating. Each frequency is focused by the cylindrical lens onto its focal plane, where the SLM is placed. At the SLM plane, $y = f\theta(\omega) = \alpha f\omega$. Thus, the phase pattern loaded on the SLM can be expressed in different coordinates as

$$\varphi(x,y) = \varphi(x,\alpha f\omega) = \varphi[x,\alpha f(\omega_0 - 2at/\tau^2)] = \varphi(x,\beta t), \tag{3}$$

where $\beta = -2\alpha f a/\tau^2$. Thus, immediately after the beam shaper, the output field can be expressed as

$$E_o(x,y,z,t) = u(x,y)A(t)e^{i(\omega_0 t-kz)}e^{-t^2/\tau^2}e^{-iat^2/\tau^2}e^{i\phi(x,\beta t)}. \tag{4}$$

Consequently, the phase pattern loaded to the SLM is directly mapped to the ST coordinates with a linear scaling factor that is determined by the grating dispersion, the input pulse width, chirp coefficient, and the cylindrical lens focal length. In the above derivation, the phase to be mapped should be a small perturbation compared with the chirp in order for the mapping picture to be accurate.

3. RESULTS

The working principle and its experimental implementation are illustrated in Fig. 1. A positively chirped pulse enters the STWP generator (pulse shaper). Each frequency component sees the corresponding modulation within the spatial phase pattern displayed on the SLM. After the pulse shaper, the reconstituted wavepacket contains the phase pattern in the ω-x plane on the SLM mapped to the t-x plane as Eq. (4).

To validate the space-to-time mapping technique, we first study the generation of STOV using the experimental setup shown in Fig. 1. Ultrashort pulses from a home-built mode-locked Yb:fiber laser are used as the input to the STWP generator. The laser emits pulses with a pulse duration of 3 ps, a center wavelength of 1030 nm, and a repetition rate of 32 MHz. The pulse coming out of the fiber laser is positively chirped. After the pulse compressor in the reference arm shown in Fig. 1, the pulse is compressed to 100 fs. In the STWP generator, in addition to the STOV phase of $l\theta_{x-\omega}$ (l is the topological charge of the helical phase, $\theta_{x-\omega}$ is the spatial-spectral azimuthal angle), different amounts of chirp can be loaded to the SLM to investigate the effects of chirp on the generated STOV wavepacket. Since the original pulse is already positively chirped, an additional quadratic phase $\phi(x,\omega) = \mathrm{GDD}\cdot(\omega-\omega_0)^2$ displayed on the SLM starts with a zero group delay dispersion (GDD) coefficient to negative GDD coefficient. The results are presented in Figs. 2 and 3. Figure 2 shows the ST intensity distribution of the generated STOV wavepackets under different chirp conditions (positive chirp, zero chirp, and negative chirp). The experimental results have a good agreement with numerical simulation results. Figure 3 shows the measured and simulated phase profiles of the STOV wavepacket when the overall GDD is positive and negative.

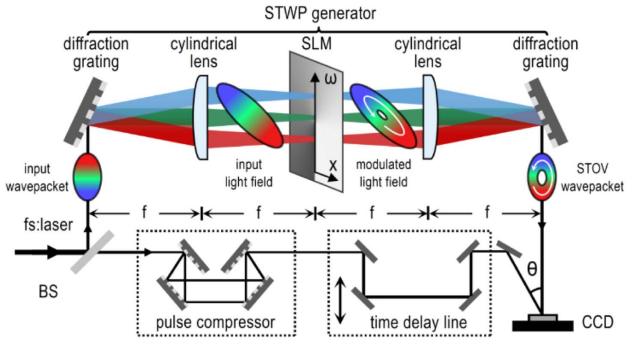

Fig. 1. Schematic of STWP generator and 3D wavepacket characterization. The experimental setup for generating and characterizing STWP. The upper arm is an STWP generator, which applies an x-ω phase to an input wavepacket. A positively chirped Gaussian–Gaussian wavepacket is modulated by a two-dimensional phase on the x-ω plane and transformed into the desired wavepacket. A helical phase pattern is used as an example for the generation of STOV. The tilt of the pulse is used to illustrate different arrival times for different frequency components. The lower arm of the setup is a reference arm that delivers a compressed probe pulse to characterize the generated STWP from the upper arm. Two wavepackets overlap on the CCD with an incident angle offset of θ. By scanning their relative time delay, 3D intensity and phase profiles of the STWP can be retrieved [9].

The measured phase shown in Fig. 3 clearly demonstrated the STOV features. When the negative GDD compensates the positive chirp from the input pulse, transform limited pulse is created [Figs. 3(c1), 3(c2) and 3(d1), 3(d2)], and the STOV wavepackets actually turn into several lobes in the ST domain as opposed to donut shapes. This also agrees well with the observation by Hancock *et al.*, where the input pulse is unchirped [12].

What is more interesting is the case when the total chirp becomes negative. This represents a frequency swapping in the time domain, meaning that the leading edge of the pulse now carries higher frequency, and its trailing edge carries lower frequency. Since the phase modulation is registered with the instantaneous frequency, this should lead to a reversal of

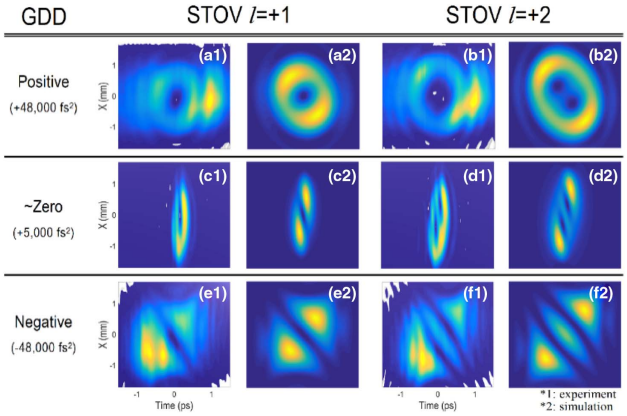

Fig. 2. ST intensity of STOV wavepackets with different amounts of GDD. The STOV wavepacket is characterized at 85 cm after the STWP generator. With different amounts of GDD added, STOV wavepackets exhibit different ST intensity profiles. The wavepacket has a ring-like intensity pattern when GDD is positive. When STOV wavepacket has a negative GDD, the ST intensity profile is distorted because of the astigmatism between dispersion and diffraction. (a), (c), (e) STOV wavepackets with a charge of $l = +1$. (b), (d), (f) STOV wavepackets with a charge of $l = +2$.

polarity for the STOV. Such an STOV polarity reversal is confirmed with the results shown in Figs. 2(e1), 2(e2), 2(f1), 2(f2), 3(c1), 3(c2), 3(d1), and 3(d2). Note how the intensity asymmetry caused by the asymmetrical spectrum from the fiber laser is swapped from the leading edge to the trailing edge of Figs. 2(a1)–2(e1) and 2(b1)–2(f1). The corresponding phase patterns are summarized in Fig. 3. Phase measurements corresponding to the intensity profile shown in Figs. 2(c1) and 2(d1) cannot be done, as the object pulse width is the same as the probe pulse width, and resolving the phase in the 3D reconstruction is very challenging. Comparing the phase patterns for positively chirped and negatively chirped pulses, clear polarity reversal of STOVs is observed, meaning the transverse OAM carried by the STOV wavepacket has reversed its orientation. The excellent agreement between the experimental results and theoretical predictions clearly validates the correspondence between the phase pattern loaded to the SLM and the spectral content of the wavepacket.

This space-to-time mapping concept further enables us to generate much more complex STWPs that are not intuitive with the other existing techniques. As examples, an ST lattice containing multiple STOVs with different topological charges arranged at different spatial and temporal coordinates is generated. The measured ST intensity and phase distributions are also shown in Fig. 4. This would be very difficult to realize with the traditional Fourier-transform-based analysis.

To further show the power of this technique, we demonstrate the collision of two STOVs in the ST domain. Two STOVs separated in time are generated first. On top of the individual STOV phase, linear phase with opposite slope is applied to each of the STOVs. The linear phase represents different time delay. Thus, we can delay the leading STOV, accelerate the trailing STOV, and observe how they approach, collide with and separate from each other. Both experimental and numerical simulation results are summarized in Fig. 5. Excellent agreements between experimental results and numerical simulation are obtained. Note that vertical fringes are observed during the collision process. These are due to the beating between different frequency contents carried by the two STOVs. Prior to the collision, broader fringes [Figs. 5(a1), 5(b1), 5(f1), and 5(g1)] are observed, while much denser fringe patterns are observed after the two STOVs passing each other [Figs. 5(d1), 5(e1), 5(i1), and 5(j1)]. This is another manifestation of the frequency to time relationship, and the denser fringes come from larger frequency difference.

The ST phase during the collision process is numerically simulated. Reliable reconstruction of the phase during this process is challenging to our current setup limited by the width of the probe pulse. However, considering the good agreement

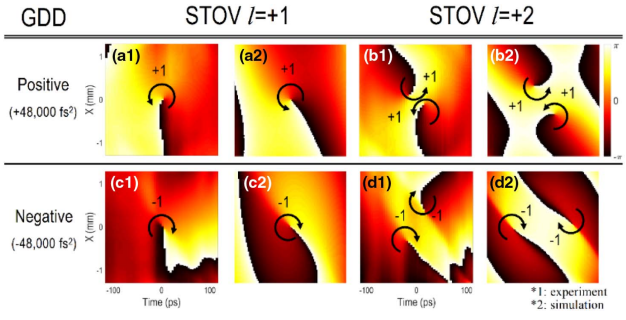

Fig. 3. ST phase profile of STOV wavepackets with different amounts of GDD. ST phase is measured for the STOV wavepackets with different GDD. The ST phase has a topological charge with opposite sign when different GDD is imposed to the wavepacket. When overall GDD is positive, the STOV charge aligns with the added ST spiral phase. Conversely, when overall GDD is negative, the STOV charge has a reversed sign. (a), (c) STOV wavepackets with an applied STOV charge of $l = +1$. (b), (d) STOV wavepackets with an applied STOV charge of $l = +2$.

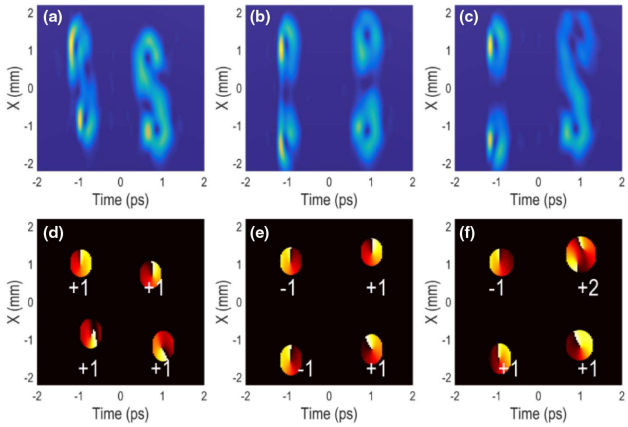

Fig. 4. STOV lattice with multiple STOVs multiplexed in space and time. (a) Four elemental ($l = +1$) STOV wavepackets in space and time. (b) Four elemental STOV wavepackets with alternating STOV polarity. (c) Four STOV wavepackets with different STOV charge ($l_1 = -1$, $l_2 = +2$, $l_3 = l_4 = +1$). (d)–(f) Corresponding measured ST phase profiles of spatiotemporally multiplexed STOV wavepackets.

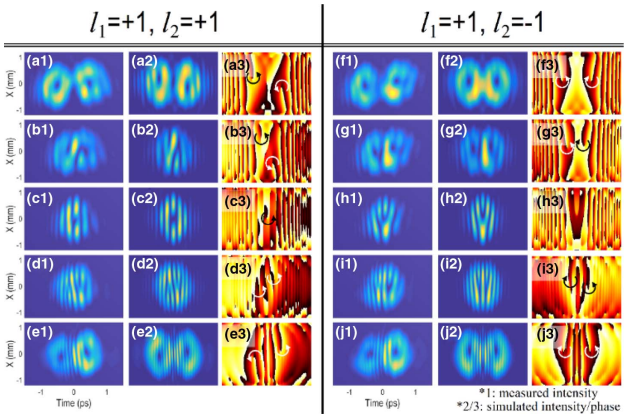

Fig. 5. ST collision of two STOVs. Linear phases with opposite signs are applied on the left/right side of the input light field to advance/delay input wavepackets in the corresponding time domain. The phase is expressed as $\phi(\omega) = k_t|\omega - \omega_0|$. Subplots (a)–(e) show the collision of two STOVs with same STOV charge $l_1 = l_2 = +1$. From (a1) to (e1), the linear phase coefficient k_t changes from −450 fs to +450 fs. Subplots (f)–(j) show the collision of two STOVs with different STOV charges $l_1 = +1$ and $l_2 = -1$.

between the intensity patterns for the experimental and numerical results, we believe that the phase patterns generated from simulation results reflect the actual ST phase in the experiment. Clear difference for the collision of two +1 STOVs and the collision between +1 and −1 STOVs can be observed. Here, we refer to the collision of two STOVs with opposite charge as STOV annihilation. It should be noted that, for the collision between +1 and −1 STOVs, they do not completely annihilate each other in the phase due to the fact that the two STOVs have different center frequency. However, the total ST OAM would be zero within this wavepacket if the spectrum distribution of the source pulse is uniform. This is similar to their spatial OAM counterparts. If two spatial OAM modes with opposite topological charges propagating in slightly different directions are superimposed together, similar interference fringes will happen in the spatial domain as well.

4. CONCLUSION

In summary, we demonstrate a space-to-time mapping pulse sculpturing technique with chirped pulses. The space-to-time mapping is understood with the spontaneous frequency of the pulse and their corresponding arrival time at the SLM within a typical 4-f pulse shaper. Such a technique opens tremendous opportunities for sculpturing wavepackets with complex ST structures such as multiple STOVs and the STOV lattice and further enables us to study the manipulations, operations, and interactions of these complex ST structures, all with a very simple yet extremely flexible and powerful STWP generator. We believe that these complex wavepackets may find use in unique applications. Finally, we want to emphasize that the scheme reported here can be readily adapted for the other spectral regimes as well as many other fields that involve wave phenomena (such as electron beams, X-rays, and acoustic waves), opening opportunities for the study and applications of different types of STWPs in a wide range of areas.

Funding. Natural Science Foundation of Shanghai (20ZR1437600); Science and Technology Commission of Shanghai Municipality (19060502500); National Natural Science Foundation of China (61805142, 61875245, 92050202).

Acknowledgment. Q. Z. proposed the original idea, performed the theoretical analysis, and supervised the project. Q. C. performed experiments and numerical analysis. J. C., K. L., C. W., and A. C. contributed in developing the experimental method. Q. C., Q. Z., and A. C. wrote the manuscript. All authors reviewed the manuscript.

Disclosures. The authors declare no competing financial interests.

Data Availability. Data underlying the results presented in this paper are not publicly available at this time but may be obtained from the authors upon reasonable request.

Code Availability. All codes used for data analysis and simulations are available from the corresponding author upon reasonable request.

REFERENCES

1. A. M. Weiner, "Femtosecond pulse shaping using spatial light modulators," Rev. Sci. Instrum. **71**, 1929–1960 (2000).
2. S. Divitt, W. Zhu, C. Zhang, H. J. Lezec, and A. Agrawal, "Ultrafast optical pulse shaping using dielectric metasurfaces," Science **364**, 890–894 (2019).
3. S. Akturk, X. Gu, P. Gabolde, and R. Trebino, "The general theory of first-order spatio-temporal distortions of Gaussian pulses and beams," Opt. Express **13**, 8642–8661 (2005).
4. H. Vincenti and F. Quéré, "Attosecond lighthouses: how to use spatiotemporally coupled light fields to generate isolated attosecond pulses," Phys. Rev. Lett. **108**, 113904 (2012).
5. D. Kim and P. T. C. So, "High-throughput three-dimensional lithographic microfabrication," Opt. Lett. **35**, 1602–1604 (2010).
6. A. Chong, W. H. Renninger, D. N. Christodoulides, and F. W. Wise, "Airy–Bessel wave packets as versatile linear light bullets," Nat. Photonics **4**, 103–106 (2010).
7. H. K. Kondakci and A. F. Abouraddy, "Diffraction-free space-time light sheets," Nat. Photonics **11**, 733–740 (2017).
8. A. Sainte-Marie, O. Gobert, and F. Quéré, "Controlling the velocity of ultrashort light pulses in vacuum through spatio-temporal couplings," Optica **4**, 1298–1304 (2017).
9. D. H. Froula, D. Turnbull, A. S. Davis, T. J. Kessler, D. Haberberger, J. P. Palastro, S.-W. Bahk, I. A. Begishev, R. Boni, S. Bucht, J. Katz, and J. L. Shaw, "Spatiotemporal control of laser intensity," Nat. Photonics **12**, 262–265 (2018).
10. B. Bhaduri, M. Yessenov, and A. F. Abouraddy, "Anomalous refraction of optical spacetime wave packets," Nat. Photonics **14**, 416–421 (2020).
11. A. Chong, C. Wan, J. Chen, and Q. Zhan, "Generation of spatiotemporal optical vortices with controllable transverse orbital angular momentum," Nat. Photonics **14**, 350–354 (2020).
12. S. Hancock, S. Zahedpour, A. Goffin, and H. Milchberg, "Free-space propagation of spatiotemporal optical vortices," Optica **6**, 1547–1553 (2019).
13. C. Wan, J. Chen, A. Chong, and Q. Zhan, "Generation of ultrafast spatiotemporal wave packet embedded with time-varying orbital angular momentum," Sci. Bull. **65**, 1334–1336 (2020).